UCLA
UCLA Previously Published Works

Title

Stoichiometry-controllable optical defects in Cu x In 2−x S y quantum dots for energy harvesting

Permalink

https://escholarship.org/uc/item/1rf2p722

Journal

Journal of Materials Chemistry A, 8(25)

ISSN

2050-7488

Authors

Fuhr, Addis S
Alexandrova, Anastassia N
Sautet, Philippe

Publication Date

2020-06-30

DOI

10.1039/d0ta03954c

Peer reviewed

eScholarship.org Powered by the California Digital Library
University of California

ARTICLE

Received 00th January 20xx,
Accepted 00th January 20xx

DOI: 10.1039/x0xx00000x

Stoichiometry-Controllable Optical Defects in $Cu_xIn_{2-x}S_y$ Quantum Dots for Energy Harvesting

Addis S. Fuhr,[a,b] Anastassia N. Alexandrova,[c,d]* Philippe Sautet[b,c,d]*

The large Stokes shift for $Cu_xIn_{2-x}S_y$ (CIS) quantum dots (QDs) reduces reabsorption losses in luminescent solar concentrators (LSCs). However, reabsorption still occurs due to their broad absorption spectra, which, along with below unity quantum yields, hamper device performance. The origin of these optical properties is heavily debated, and makes it difficult to optimize CIS for LSCs and other energy harvesting devices such as solid-state and sensitized solar cells. Here, we show with density functional theory calculations that anti-site defects (Cu_{In}'' + In_{Cu}••) form in near-stoichiometric CIS QDs, while copper vacancies charge-compensated by the oxidation of a second Cu atom (V_{Cu}' + Cu_{Cu}•) form in Cu-deficient structures. Both defects lead to large Stokes shifts, but Cu_{In}'' defects only localize holes in the excited-state leading to strong intragap absorption, which is suppressed for paramagnetic Cu_{Cu}• defects that localize holes in the ground-state. The relative concentration of each defect and competing defect phases that lead to non-emissive carrier trapping is controllable by stoichiometry and Fermi-level, and optimal chemical processing conditions for energy harvesting applications are discussed.

Introduction

Solar energy currently accounts for only 1.8% of the global electricity supply, but has the potential to reduce greenhouse gas emissions if its usage massively expands.[1, 2] $Cu_xIn_{2-x}Se_yS_{2-y}$ (CIS) quantum dots (QDs) are attractive materials for low-cost solar power conversion schemes. In particular, they have been used in recent Champion device quantum dot sensitized solar cells, and luminescent solar concentrators (LSCs) with photovoltaic windows.[3-6]

Despite growing interest in CIS QDs, the origin of their unusual optical properties is still elusive.[7-19] For example, CIS QDs have larger Stokes shifts (270-750 meV), broader absorption and ensemble photoluminescence (PL) emission spectra (>300 meV), and longer radiative lifetimes (100-500 ns) than II-VI QDs.[7-19] This is generally attributed to radiative recombination between a delocalized conduction band electron and a hole localized on a Cu atom via either native defects,[7-10, 13-19] or self-trapped excitons.[9, 11-12, 14] For defect emission, an interruption in the crystal lattice from an "out of place" Cu ion is expected to lead to an intragap hole localized state. The self-trapped exciton model, on the other hand, proposes that the complex shape of *d* orbitals in CIS causes poor electronic feedback and ~~an~~ inability to form delocalized valence band (VB) hole states, and results in defect-like localized *d* orbitals for "normal" lattice Cu^{1+} ions.[11-12] This leads to strong electron-phonon coupling where each Cu^{1+} state undergoes a large nuclear reorganization when photoconverted to Jahn-Teller distorted Cu^{2+}. Each of these mechanisms have successfully explained some aspects of emission. For example, Cu-containing QDs typically exhibit large Huang-Rhys factors, which is consistent with significant excited-state nuclear reorganization.[11] However, single particle PL linewidths for CIS can be as narrow as 60 meV, which is in agreement with the defect emission model.[18] To address this issue, recently it has been proposed that there are two sets of Cu defects: "Cu^{1+} defects" that undergo a self-trapped exciton-like reorganization, and "Cu^{2+} defects," which do not require excited-state reorganization.[20] Stoichiometry-dependent optical spectra confirms this interpretation, but could only hypothesize the precise chemical identity for each of these defects.[20]

Developing a clear understanding of structure-property relationships in CIS QDs is of significant importance to energy harvesting applications.[21-32] For example, a key performance limiting factor for LSCs is reabsorption, which occurs when there is spectral overlap between the fluorophore's absorption and emission.[21] These losses scale with PV window size, and the large Stokes shift of CIS QDs is advantageous for reducing reabsorption and improving LSC performance.[5-6, 21-24] Yet, these advantages are somewhat mitigated by broad spectral

[a] *Chemistry Division, Los Alamos National Laboratory, Los Alamos, New Mexico 87545, United States*
[b] *Department of Chemical and Biomolecular Engineering, University of California, Los Angeles, Los Angeles, California 90095, United States: E-Mail: sautet@ucla.edu*
[c] *Department of Chemistry and Biochemistry, University of California, Los Angeles, Los Angeles, California 90095, United States: E-Mail: ana@chem.ucla.edu*
[d] *California NanoSystems Institute, University of California, Los Angeles, Los Angeles, California 90095, United States.*

†Electronic Supplementary Information (ESI) available: See
DOI: 10.1039/x0xx00000x

Please do not adjust margins

linewidths, which if "sharpened" without losing the large Stokes shift would be beneficial for LSCs. Understanding the origin of the broad absorption spectra is also of particular importance to solid-state solar cells where Urbach tailing can reduce the open circuit voltage and limit power conversion efficiency.[26, 29-32] In addition, for both solar cells and LSCs, the formation of absorptive and/or emissive defects under different chemical processing conditions has not been studied in the context of competing secondary defect phases. These secondary structures can potentially hamper CIS QD performance in energy harvesting devices by increasing the density of non-emissive trap states, which reduce quantum yield (QY) or lead to recombination losses.[21]

In this letter, we use Density Functional Theory (DFT) calculations to identify defects that form in CIS QDs under different growth conditions, and predict their effects on optical spectra by unifying aspects of different proposed emission models. Specifically, we find that anti-site (Cu_{In}'' + $In_{Cu}^{\bullet\bullet}$) defect pairs lead to intragap absorption and emission in near-stoichiometric CIS. Cu-deficient CIS, on the other hand, has a larger concentration of copper vacancies that leads to Cu^{2+} defects (V_{Cu}' + $Cu_{Cu}^{\bullet}$), which are paramagnetic and non-absorptive due to a hole in the Cu *d* shell, ~~. Hence,~~thus resulting in intragap emission without intragap absorption. This leads to a similarly large Stokes shift as anti-site defects, but with narrower absorption spectra. Correspondingly, Cu-deficient CIS should have reduced reabsorption losses for LSCs, and weaker Urbach tailing for solar cells resulting in higher power conversion efficiencies for both energy harvesting device schemes. We also identify non-emissive competing defect phases such as $2V_{Cu}'$ + $In_{Cu}^{\bullet\bullet}$ defect pairs that reduce the density of emissive $Cu_{Cu}^{\bullet}$ defects, and isolated hole (V_{Cu}') and electron ($In_{Cu}^{\bullet\bullet}$) trapping defects that lead to nonradiative recombination. We conclude by discussing the interplay between emissive and non-emissive defect formation as a function of stoichiometry and Fermi level. ~~And,~~In addition, we discuss their corresponding implications towards optimizing the chemical process conditions and structure of CIS for different energy harvesting devices such as solid-state solar cells, sensitized solar cells, and LSCs.

Methods

Plane-wave PAW DFT calculations were performed with VASP.[33-36] CIS lattice constants and band gap were obtained by relaxing a bulk Chalcopyrite unit-cell and conducting subsequent single-point calculations using the Heyd-Scuseria-Ernzerhof (HSE06)[37] hybrid range separated exchange-correlation functional~~HSE06[37]~~ functional. Supercells and quantum dots were generated from the HSE06 relaxed bulk. The formation energy of different defects in the CIS supercell were obtained by introducing defects into the supercell, subsequent ionic relaxation using the Perdew-Burke-Ernzerhof (PBE) functional,[38] and using equation 1 from ref. 39:

$$E_{form} = E_{tot}(¿) - E_{tot}¿ \quad (1)$$

where $E_{tot}(¿) - E_{tot}¿$ represents the energy difference between defective and non-defective supercells, n_α is the number of atoms added (-1) or removed (+1) of species α and chemical potential μ_α, q represents the charge of the defect, E_F the Fermi-level, and E_{corr} the FNV correction for the effects of a finite-sized supercell on charged defect formation.[39] The chemical potential (μ_α) was determined by calculating the energy per atom (E_α^{solid}) of elemental solid α, and adding the relative chemical potential ($\Delta\mu_\alpha$) using the points marked in the CIS stability region of the chemical potential diagram from Fig. 1 ($\mu_\alpha = \Delta\mu_\alpha + E_\alpha^{solid}$). Here, a more negative $\Delta\mu_\alpha$ reflects a greater deficiency in species α ~~deficiency~~ ($\Delta\mu_\alpha = 0$ corresponds with an α-rich condition). The stability region for CIS in the chemical potential diagram was determined by calculating the formation energy of competing Copper and Indium Sulfide phases under different $\Delta\mu_\alpha$ conditions. For all stoichiometric, charge-balanced defects only the $E_{tot}(¿) - E_{tot}¿$ term is used. The correction term (E_{corr}) for the finite-size of the supercell is determined by the FNV method described in ref. 39. The magnitude of the correction term is similar to that calculated for related CISe structures (see Fig. S1 in †ESI and ref. 40). The Franck-Condon, or "True Stokes shift" was calculated via the configuration coordinate method used in ref. 39 for anti-site (Cu_{In}'' + $In_{Cu}^{\bullet\bullet}$) defect pairs $\{R\}_{q=-1} - \{R\}_{q=0}$ (Fig. 2).

All calculations used an energy cut-off of 280 eV, and the geometries were relaxed until forces were smaller than 0.05 eV/Å per atom. The HSE06 screening parameter was ω=0.13 as described in previous reports.[41-42] Integrals in the unit-cell were calculated by sampling the Brillouin zone with a 6x6x3 Monkhorst-Pack k-point grid. Defect calculations used a 2x2x2 supercell with Gamma-centered 2x2x2 k-points. QDs were calculated at the Gamma point only. Calculations with a single copper vacancy were open shell, using the MAGMOM tag to capture magnetic interactions.

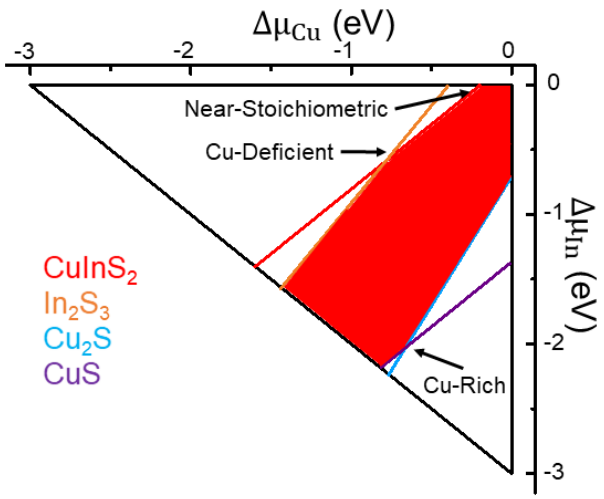

Fig. 1 Chemical potential diagram predicting the stoichiometry-dependent CIS stability region

Results & Discussion

Stoichiometry & Fermi-Level Dependent Stability of Defects

~~The~~ HSE06 ~~Heyd-Scuseria-Ernzerhof (HSE06)[37] hybrid range separated exchange-correlation functional~~ was used to calculate lattice constants and electronic structure due to its ability to accurately reproduce the electronic properties of

This journal is © The Royal Society of Chemistry 20xx

Please do not adjust margins

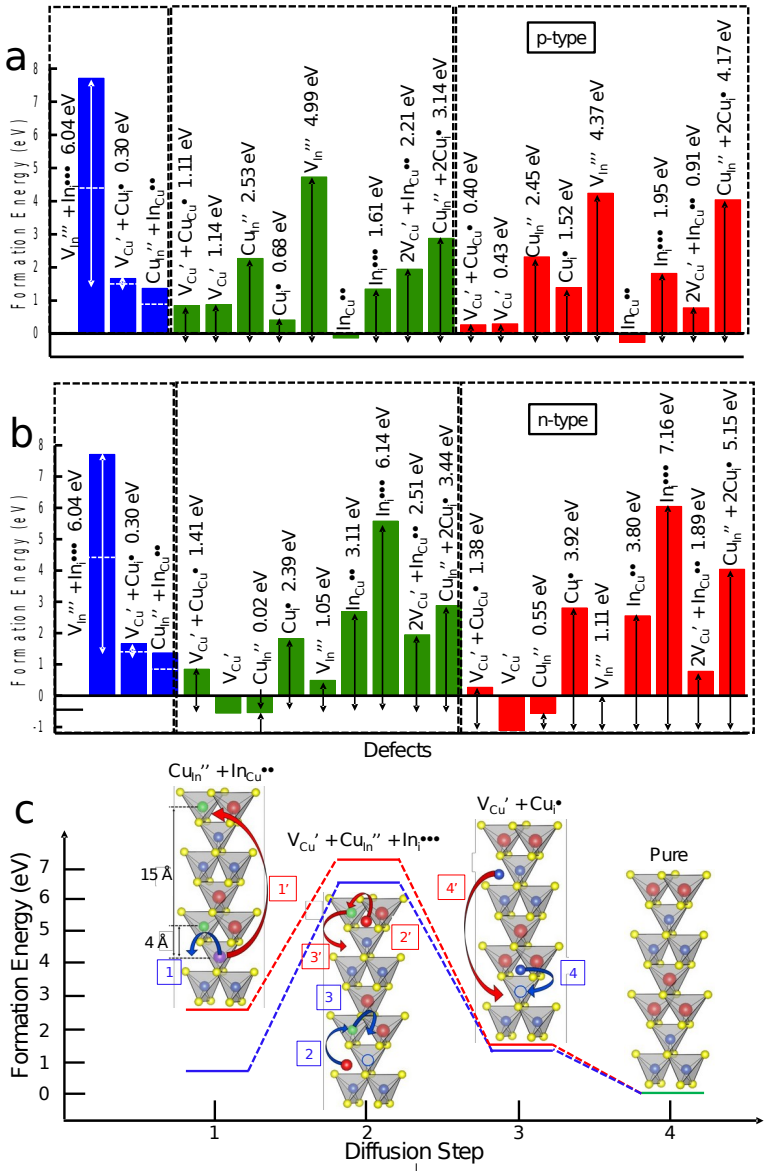

bulk semiconductors,[43] while ~~the Perdew-Burke-Ernzerhof (PBE) exchange-correlation functional~~ PBE[38] was chosen for ionic relaxations and formation energy calculations due to its lower computational expense (see methods and Fig. S2 in †ESI). The formation energy of defects and defect pairs was calculated with a 2x2x2 (128 atom) supercell in different chemical and electron potential environments (Fig. 1 and Fig. 2). Here, the relative chemical potential ($\Delta\mu_\alpha$, where α = In or Cu) is used as an indicator of "Cu-rich" or "Cu-deficient" growth conditions (see methods), and is bounded by competing Indium and Copper Sulfide phases (Fig. 1). Defect formation mechanisms were studied under stoichiometric, near-stoichiometric (slightly Cu-deficient), and Cu-deficient conditions (each marked in the phase diagram presented in Fig. 1). Supercells are used instead of a quantum dots to determine formation energies in order to negate the influence of surfaces (Fig. 1 and Fig. S3 in †ESI). This approach is justified by experimental studies, which showed that surface passivation with an alloyed ZnS shell does not significantly affect emission energy or linewidth.[15, 19] This, in addition to the similarly large Stokes shift observed in bulk CIS, suggests that it is unlikely that surface states are responsible for emission.

The charge-balanced, stoichiometric defect pairs we considered (blue bars in Fig. 2) include anti-site defects wherein Cu^{1+} and In^{3+} swap lattice positions. Cu at the In site is noted (Cu_{In}'', the primes indicating that two more electrons are placed at this site after the swap, although the Cu formal oxidation number remains +I. Similarly, In at the Cu site is noted $In_{Cu}^{\bullet\bullet}$, where ~~primes and~~ dots indicate ~~negative and positive charges~~that two more holes ~~aplced~~are placed at the site after the swap.~~, respectively~~), ~~and~~). They also include Frenkel pairs, wherein a cation vacancy forms after the cation is ejected from its normal lattice position into an interstitial space (V_{Cu}' + $Cu_i^{\bullet}$ and V_{In}''' + $In_i^{\bullet\bullet\bullet}$). For near-stoichiometric, and Cu-deficient structures, which are often used in devices,[44-46] we calculated the formation energy of each of these defects in isolation, as well as off-stoichiometry defect pairs such as Cu_{In}'' + $2Cu_i^{\bullet}$ and $2V_{Cu}'$ + $In_{Cu}^{\bullet\bullet}$ (green and red bars in Fig. 2). This introduces an electronic hole in the later described electronic structure calculations for Cu vacancies, which localizes on a Cu atom, and forms a Cu^{2+} centre for charge-compensation (V_{Cu}' +

$Cu_{Cu}^{\bullet}$). In each case, we present the formation energies as a function of the electron potential, or Fermi level (E_F), which is defined relative to the VB, and represents p- (near 0 eV, here VB + 0.026 eV or k_BT in Fig. 2a) or n-type (near the computational band gap of 1.47 eV, here CB - 0.026 eV or k_BT in Fig. 2b) environments.

The formation energies for each defect pair decreases at shorter separation distances due to charge stabilization (Fig. S3 in †ESI shows the distance-dependent energies, the blue bars in Fig. 2 shows their average, and the white dashed lines mark their lowest energy). Anti-site defects have the lowest average formation energy under stoichiometric conditions. At close (< 0.5 nm) separation distances (Fig. 2 and Fig. S3 in †ESI) anti-site defect pairs have similar formation energies as $V_{Cu}' + Cu_{Cu}^{\bullet}$ (ΔE for $In_{Cu}'' + In_{Cu}^{\bullet\bullet}$ is ~ 0.03 eV > $V_{Cu}' + Cu_{Cu}^{\bullet}$). This suggests that under stoichiometric conditions anti-site defect pairs form in the largest concentrations, but under mildly Cu-deficient, or near-stoichiometric conditions, are close in energy with $V_{Cu}' + Cu_{Cu}^{\bullet}$ defects. Under highly Cu-deficient conditions, however, $V_{Cu}' + Cu_{Cu}^{\bullet}$ form in the largest concentration. We test their stability by calculating the formation energy of several intermediate defect structures required for back-diffusion into the original lattice sites, or "self-purification" (Fig. 2c). These states have high formation energies, and the defects studied here are likely kinetically trapped during synthesis.

Fermi-level (E_F) has a significant impact on the formation of competing defect phases. Under more p-type conditions (Fig. 2a) isolated copper vacancies have formation energies slightly higher than the $V_{Cu}' + Cu_{Cu}^{\bullet}$ defect pair (ΔE for V_{Cu}' is ~ 0.03 eV > $V_{Cu}' + Cu_{Cu}^{\bullet}$) indicating that while the formation of "Cu^{2+}" defects, or the $V_{Cu}' + Cu_{Cu}^{\bullet}$ defect pair is favourable, a similarly high density of isolated copper vacancies should also form in CIS. If E_F is closer to the CB (n-type conditions), isolated V_{Cu}' have a much lower formation energy (difference of ~1.38 eV) than the $V_{Cu}' + Cu_{Cu}^{\bullet}$ defect pair. For isolated anti-site defects, low E_F (p-type) conditions strongly favour $In_{Cu}^{\bullet\bullet}$ whereas high E_F (n-type) conditions strongly favour Cu_{In}''. Interestingly, while Frenkel pairs have significantly higher formation energies than anti-site defect pairs, under p-type conditions the formation energy of copper interstitials ($Cu_i^{\bullet}$) appears to be ~0.43 eV lower than the $V_{Cu}' + Cu_{Cu}^{\bullet}$ defect pair for near-stoichiometric CIS. For n-type conditions in near-stoichiometric CIS, indium vacancies (V_{In}''') ~~are~~ have similarly low formation energy (~0.36 eV lower than $V_{Cu}' + Cu_{Cu}^{\bullet}$ defects), which indicates that the formation of both sets of isolated defects may affect optical transitions. Indium interstitials, on the other hand, have universally high formation energies and are therefore are unlikely to form in CIS. These trends also hold for Cu-rich processing conditions (Fig. S4 in †ESI), but with generally lower formation energies for isolated Cu_{In}'', V_{In}''', and $Cu_i^{\bullet}$ defects, and higher formation energies for isolated V_{Cu}', $In_{Cu}^{\bullet\bullet}$ defects.

Impact of Defects on Spectral Shape

The density of states (DOS) for a CIS supercell with anti-site defect pairs (Fig. 3a, left panel) has an occupied intragap state (centered on Cu_{In}'') below E_F whereas the DOS for a CIS supercell with a copper vacancy (Fig. 3a, right panel) has an unoccupied spin-polarized state (centered on $Cu_{Cu}^{\bullet}$) above E_F. The energy difference between the VB and defect (372 and 210 meV, respectively) is close to the experimental Stokes shift (Δ_S)[7-20] and indicates that both Cu_{In}'' and $Cu_{Cu}^{\bullet}$ defects in CIS QDs lead to large Δ_S, but via different hole localization mechanisms. This was first proposed in ref. 20, which experimentally detected the presence of "Cu^{1+}" and "Cu^{2+}" defects in CIS QDs. Our calculations agree with this interpretation, and attach clear chemical identities to these defects. This is further explored by computing the theoretical absorption spectra (Fig. 3b) using linear response theory and equations 2 and 3:

$$\kappa(\omega)=\sqrt{\frac{\sqrt{\varepsilon_1(\omega)^2+\varepsilon_2(\omega)^2}-\varepsilon_1(\omega)}{2}} \quad (2)$$

$$\alpha(\omega)=\frac{4\pi}{\lambda}\kappa(\omega) \quad (3)$$

where the linear absorption coefficient (α) is determined via calculating the real $\varepsilon_1(\omega)$ and imaginary $\varepsilon_2(\omega)$ parts of the frequency-dependent dielectric constant. The excitonic transition energies ($h\upsilon_{x,a}$ in Fig. 3a,b) are identical and near the predicted band gap (~1.5 eV) for both structures. However, if CIS has Cu_{In}'' defects, there is a second lower energy transition ($h\upsilon_{Cu,a}$ in Fig. 3a,b) due to localization of a VB hole to a Cu_{In}'' (Cu^{1+} in ref. 20) state, and excitation of an intragap electron from Cu_{In}'' to the conduction band (CB). CIS QDs with Cu vacancies V_{Cu}', conversely, have a ground-state hole in d band ($Cu_{Cu}^{\bullet}$, Cu^{2+} in ref. 20), which instead captures a VB electron in an IR transition (Fig. S5 in †ESI).

These computational predictions imply distinct spectroscopic signatures for each defect, and a link between defect type and stoichiometry. Specifically, the *d* shell for Cu_{In}'' is filled with electrons ($[Ar]3d^{10}$) and more frequently form in (near)-stoichiometric or Cu-rich CIS whereas the *d* shell for $Cu_{Cu}^{\bullet}$ ($[Ar]3d^{9}$) has a hole, and forms in larger concentrations in Cu-deficient structures to charge compensate V_{Cu}'. Transient absorption (TA) spectroscopy has detected the presence of "Cu^{1+}" defects (Cu_{In}''), and confirmed our predictions whereby Cu-rich (mostly Cu_{In}'') and near-stoichiometric CIS QDs (similar Cu_{In}'' and $Cu_{Cu}^{\bullet}$ depending on the exact Cu:In) have broader spectra than Cu-deficient (more $Cu_{Cu}^{\bullet}$) structures due to strong overlap between $h\upsilon_{Cu,a}$ and $h\upsilon_{x,a}$.[20] The strength of $h\upsilon_{Cu,a}$ decreases with increasing Cu-deficiency until eventually the spectral shape evolves into a Bi-Gaussian with a strong $h\upsilon_{x,a}$ bleach and weak $h\upsilon_{Cu,a}$ shoulder.[20] As the concentration of V_{Cu}' grows, ~~the strength of~~ the VB electron → $Cu_{Cu}^{\bullet}$ hole IR transition also becomes stronger, but is outside of the detection range of typical TA experiments, and obscured in FTIR measurements by molecular vibrations of similar energy from surface passivating ligands. However, $Cu_{Cu}^{\bullet}$ centers also lead to dilute magnetic semiconductor (DMS) characteristics, which have been experimentally detected in magnetic circular dichroism (MCD) experiments.[20] Specifically, Zeeman splitting increases due to stronger spin-exchange (E_{EXCH}), and is proportional to the concentration of paramagnetic defects.[17, 20, 47-49] The simultaneous decrease in TA linewidth and increase in E_{EXCH} for more Cu-deficient

This journal is © The Royal Society of Chemistry 20xx

Please do not adjust margins

structures is indicative that Cu_{In}'' ($hu_{Cu,a}$ and no DMS characteristics) are being replaced by Cu_{Cu}• (DMS characteristics and no $hu_{Cu,a}$),[20] thus, confirming our computational predictions.

required to transiently stabilize the photogenerated hole.[11,12, 20, 51] We therefore calculate the Franck-Condon shift (δ_0) for anti-site defects (Cu_{In}'' → Cu_{In}' in Fig. 3c,d), which is 107 meV (see methods).

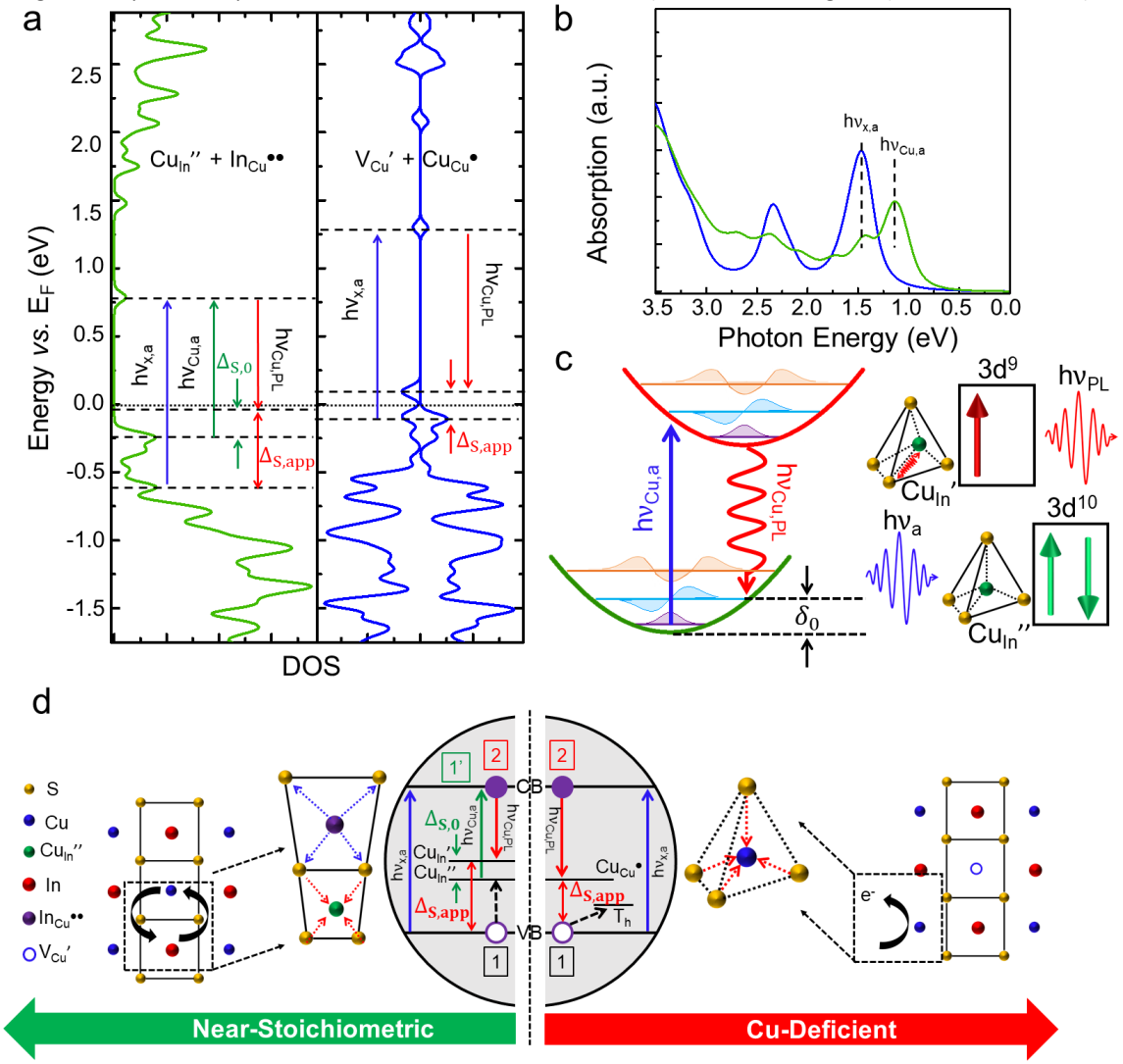

Fig. 3 (a) DOS for CIS supercells with Cu defects. Copper vacancies lead to a spin polarized intragap "Cu^{2+}" state (right) whereas anti-site defects lead to an intragap "Cu^{1+}" state (left). The predicted optical transitions are shown in coloured arrows ~~using the notation from ref. 20~~. (b) Computed linear absorption spectra for the DOS in (a). (c) Schematic depiction of the calculated "True Stokes shift", or $\Delta_{S,0}$ in (a), which is due to a Jahn-Teller distortion in excited-state Cu ($\Delta_{S,0} \neq 2\delta_0$). (d, left panel) Anti-site defects lead to intragap absorption ($h\upsilon_{Cu,a}$) in addition to band-edge absorption ($h\upsilon_{x,a}$). This causes a "True" Stokes shift (energy difference between $h\upsilon_{Cu,a}$ - $h\upsilon_{Cu,PL}$) and an "Apparent" Stokes shift (energy difference between $h\upsilon_{x,a}$ - $h\upsilon_{Cu,PL}$). (d, right panel) QDs with copper vacancies only have an "Apparent Stokes shift."

Holes (captured from the VB) transiently localize to Cu_{In}'' in the excited state (Fig. 3c and the left panel of Fig. 3d) whereas they are localized in the ground state for Cu_{Cu}•. In the latter case, VB holes are removed by a second defect (here, isolated V_{Cu}' as calculated in Fig. 2 and Fig. 4) or surface state (T_h in the right panel of Fig. 3d and ref. 20), which prevents transitions faster than defect emission such as trion decay or band-edge recombination.[19, 20] Band-edge emission can only occur in defect-free structures, which have not been synthesized to date.[13, 50] Notably, hole localization for Cu_{In}'' is similar to the self-trapped exciton model, and even though we expect band-edge absorption ($hu_{x,a}$) to occur in conjunction with defect absorption ($hu_{Cu,a}$), an electron-phonon coupled excited-state nuclear reorganization similar to Jahn-Teller distorted Cu^{2+} is

This corresponds with an emission shift of 214 meV ($\Delta_{S,0} = 2\delta_0$). Consistent with ref. 20, we label the resulting shift in emission the "True Stokes shift" ($\Delta_{S,0}$) in Fig. 3a and the left panel of Fig. 3d), which reflects the energy difference between ground-state (Cu_{In}'') and excited-state (Cu_{In}') anti-site defects ($hu_{Cu,a}$ and $hu_{Cu,PL}$ in Fig. 3c). This also leads to a larger "Apparent Stokes shift" reflecting the energy separation between band-edge absorption and emission from excited-state anti-site defects ($hu_{x,a}$ and $hu_{Cu,PL}$ in Fig. 3d). Here, our calculated True Stokes shift is 214 meV ($\Delta_{S,0} = 2\delta_0$) and Apparent Stokes shift 586 meV, which are similar to experimental measurements for "Cu^{1+}" defects (210 meV and 420 meV, respectively).[20] CIS QDs with Cu_{Cu}• only exhibit the "Apparent Stokes shift" as the ground-state defect is already Jahn-Teller

Please do not adjust margins

distorted (right panel of Fig. 3d). Removal of the "True Stokes shift" in Cu-deficient structures "sharpens" linear absorption spectra, and reduces overlap with emission.

Competing Defect Phases, Optical Losses, & Device Implications

In order to better understand how competing defect formation mechanisms can affect optical losses, we compare their formation energies and charge transition levels under different chemical processing conditions (Fig. 4). The chemical potentials used for "near-stoichiometric" and "Cu-deficient" conditions are the same as described in Fig. 1 and Fig. 2. Cu-rich conditions are shown in Fig. S4 (†ESI). Copper vacancies have low formation energies for all fermi-level values in near-stochiometric and Cu-deficient structures. Their expected charge transition (1-/0) is near the VB (VB + 0.03 eV) making them shallow hole traps. However, spectral electrochemistry studies have found that while both "Cu^{1+}" (Cu_{In}'') and "Cu^{2+}" ($Cu_{Cu}^{\bullet}$) defect emission can be quenched by electron traps, hole traps do not quench emission for Cu^{2+} defects, which are already "emission ready" and do not require excited-state hole localization due to the ground-state hole in the Cu^{2+} *d* shell.[15] Hence, a high density of isolated copper vacancies should only reduce emission efficiency for near-stoichiometric CIS, which have Cu_{In}'' defects that require photoactivation by a VB hole prior to emission.

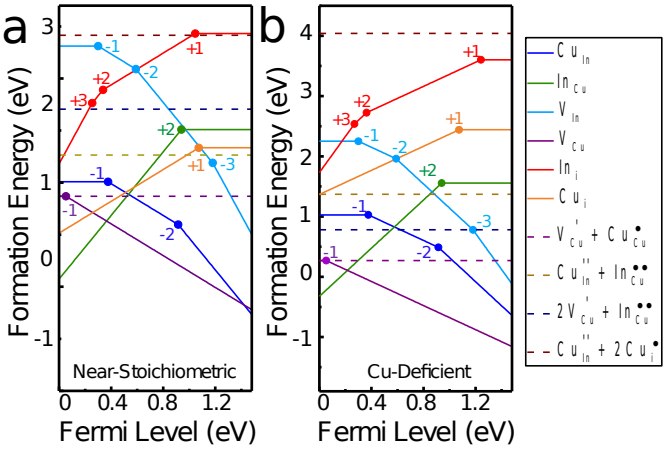

Fig. 4 (a,b) Formation energy of different defects as a function of the Fermi level energy under near-stoichiometric and Cu-deficient conditions, which are calculated at their corresponding points in the CIS stability diagram marked in Fig. 1. The closed circle symbols indicate the charge transition levels.

Under low E_F conditions, $In_{Cu}^{\bullet\bullet}$ defects have the lowest formation energy of all defects for both Cu-deficient and near-stoichiometric CIS making them likely to form in both structures. The formation of copper interstitials, on the other hand, is strongly dependent on stoichiometry, and these are not likely to form in Cu-deficient structures due to high formation energies. Both defects can act as relatively deep electron traps. The double-electron charge transition level for $In_{Cu}^{\bullet\bullet}$ defects (2+/0) and single electron charge transition level for $Cu_i^{\bullet}$ defects are CB-0.53 eV and CB-0.40 eV, respectively. However, even for very low E_F and near-stoichiometric conditions, the formation energy for $In_{Cu}^{\bullet\bullet}$ is significantly lower than that of $Cu_i^{\bullet}$ defects, and we expect $In_{Cu}^{\bullet\bullet}$ defects to have a more significant impact on electron-trap mediated nonradiative recombination for all conditions other than Cu-rich CIS where $In_{Cu}^{\bullet\bullet}$ have much higher formation energies (Fig. S4 in †ESI). Moreover, at intermediate E_F where $Cu_i^{\bullet-}$ and $In_{Cu}^{\bullet\bullet-}$ have more comparable formation energies, the Cu_{In}'' state is significantly lower in energy than $Cu_i^{\bullet}$, while indium vacancies (V_{In}''') simultaneously have very large formation energies. Hence, it is likely that even under these conditions Cu interstitials do not form in high concentrations, and instead act as metastable intermediate defect states that facilitate the diffusion of a Cu^{1+} ion into an indium vacancy to stabilize it by forming a Cu_{In}'' defect state. For both $Cu_i^{\bullet}$ and $In_{Cu}^{\bullet\bullet}$ it is unlikely that these transition energies correspond with emission as it has been well-established experimentally that emission in CIS arises from localized hole and delocalized electron states, which indicates that electron localizing defects act as optical traps that limit emission efficiency.[9, 15-16, 19] Indeed, experimentally it has been observed that the primary deactivation mechanism for CIS emission is electron trapping, which is consistent with our prediction of a high density of $In_{Cu}^{\bullet\bullet}$ defects.[15-16, 19]

As E_F moves closer to the CB, hole trapping defects are expected to contribute more to optical losses. Specifically, the formation energy of isolated vacancies (V_{Cu}' and V_{In}''') decreases at high E_F, and both shallow (1-/0) = VB+0.03 eV and deep (3-/2-) = VB+0.30 eV acceptor levels form for copper and indium vacancies, respectively. As mentioned earlier, this should significantly reduce the emission efficiency for near-stoichiometric and Cu-rich CIS, which have anti-site defects that require excited-state hole localization prior to emission, but is not expected to contribute to optical losses for Cu-deficient CIS where $Cu_{Cu}^{\bullet}$ defects are "emission ready" in the ground state, and hole trapping defects actually aid emission by blocking the faster band-edge or positive trion recombination pathways. Indium vacancies have high formation energies in Cu-deficient structures, while copper vacancies have low formation energies under both near-stoichiometric and Cu-deficient conditions. It is therefore expected that this VB hole removal process for the $Cu_{Cu}^{\bullet}$ defect emission in Cu-deficient structures only occurs via copper vacancies and not indium vacancies. However, both copper and indium vacancies can contribute to hole trapping mediated nonradiative recombination losses for anti-site defects in near-stoichiometric or Cu-rich structures.

A natural prediction from these findings would be that highly Cu-deficient structures are always ideal for improved LSC and solar cell performance as Cu-deficiency facilitates the formation of $Cu_{Cu}^{\bullet}$ defects, leads to higher QY and reduced nonradiative recombination losses due to a decrease in hole trapping, reduced band-tailing corresponding with a higher open circuit voltage in solar cells, and reduced reabsorption losses for LSCs. However, the formation energy of isolated $In_{Cu}^{\bullet\bullet}$ defects, and $2V_{Cu}' + In_{Cu}^{\bullet\bullet}$ defect pairs *also* decrease as CIS is made more Cu-deficient (Fig. S6 in †ESI), which eventually lowers QY by either reducing the density of $Cu_{Cu}^{\bullet}$ defects via competition from the $2V_{Cu}' + In_{Cu}^{\bullet\bullet}$ defect pair, or by an increase in the concentration of electron trapping $In_{Cu}^{\bullet\bullet}$ defects. Hence, decreasing the Cu:In ratio will initially improve LSC and solid-state solar cell performance by reducing reabsorption, band tailing, and nonradiative recombination losses, but eventually further narrowing of the absorption spectra will coincide with an increase in optical trap density, and will lead to larger nonradiative recombination losses for highly Cu-deficient structures. Hence, moderately Cu-deficient structures will generally be "ideal," but the exact Cu:In ratio will somewhat vary by synthetic methodology due

This journal is © The Royal Society of Chemistry 20xx

Please do not adjust margins

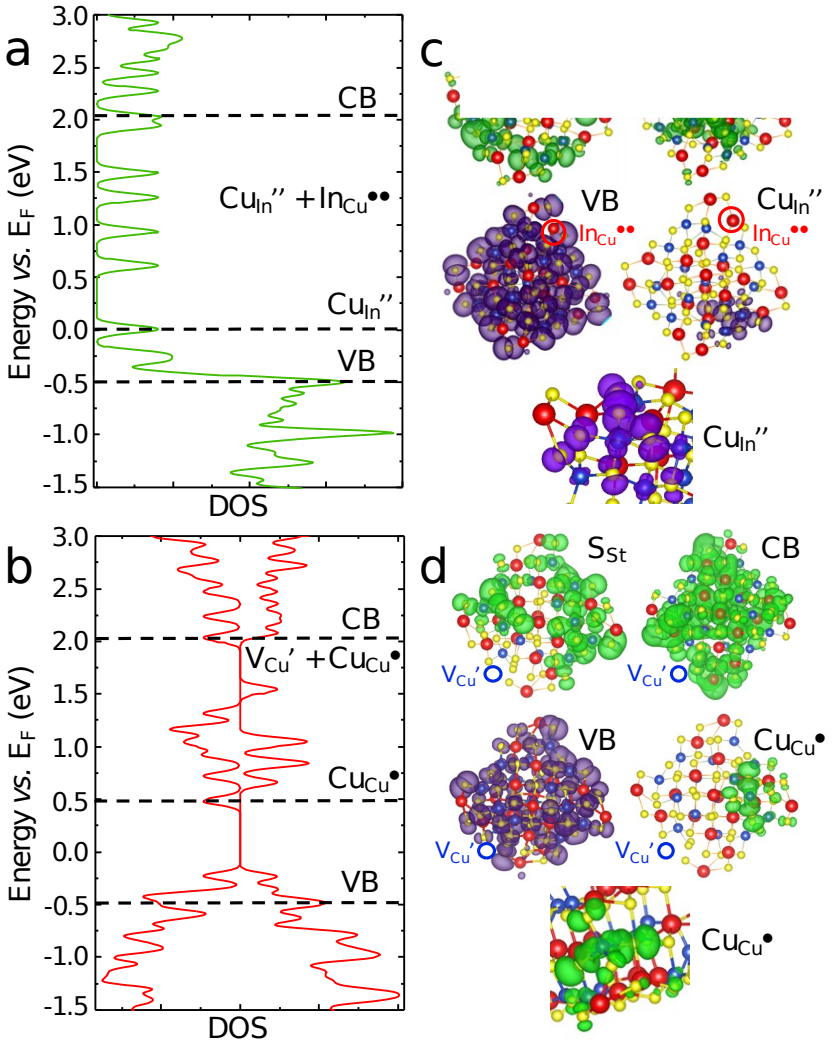

to the fact that kinetic trapping strongly affects defect formation (Fig. 2). Indeed, the presence of $2V_{Cu}' + In_{Cu}^{\bullet\bullet}$ defect pairs has also been evidenced by Raman spectroscopy,[38] and experimental QY is generally highest for moderately Cu-deficient structures.[7, 20] Lastly, for sensitized solar cells, Cu-rich CIS should be ideal. Similar to solid-state solar cells, intragap absorption from anti-site defects can lead to larger open-circuit currents, but unlike solid-state solar cells this will occur without negatively impacting the open-circuit voltage, which is pinned by the energy difference between the excited-state anti-site defect hole and delocalized CB electron due to ultrafast hole capture.[20]

In order to confirm the localized/delocalized nature of these predicted transitions in QDs, we calculate the DOS (Fig. 5) for CIS QDs with anti-site defects and copper vacancies (see methods). We confirm the identity of each state by plotting iso-energetic contours (purple and green for occupied and unoccupied energy levels, respectively) of the associated charge density (square modulus of the one electron wavefunction), similar to other reports.[52-55] We define surface states (S_{St}) as delocalized across surface atoms, and defect states (Cu_{In}'' and $Cu_{Cu}^{\bullet}$) as localized to the intentionally created defect coordination sphere. However, the S_{St} contribution to the DOS is overestimated here due to our inability to include passivation layers of native ligands (*e.g.* dodecanethiol), which would increase computational expense. Indeed, this is why we computed the absorption spectra for CIS using supercells without dangling bonds. The Cu_{In}'' state is occupied (below E_F), and therefore absorptive and not paramagnetic whereas $Cu_{Cu}^{\bullet}$ is above E_F, paramagnetic, and not absorptive. The predicted energy separation between Cu_{In}'' and $Cu_{Cu}^{\bullet}$ versus the VB (~590 meV and 740 meV, respectively) are of similar magnitude to our supercell calculations. In addition, the position of the defect affects its energy versus the band-edges (Fig. S7), and Δ_S is impacted by the local defect bonding environment as expected by single-particle spectroscopy studies on CIS QDs, and DFT studies on related Cu-doped ZnSe QDs.[18, 56] Moreover, the band-edges are delocalized, and we expect both delocalized and localized transitions to occur.

The similarity between the supercell and QD calculations confirms that the nature of the optical transitions between bulk and QD systems is similar. A clear distinction between the two mechanisms is the larger contribution of surface states to optical deactivation mechanisms for QDs in comparison to the bulk. Specifically, QDs have non-surface bulk-like defects that affect absorption, emission, and nonradiative recombination mechanisms, but also have *additional* optical traps due to dangling bond surface states. Based on the calculated DOS, these dangling bond surface states are expected to mostly be electron traps as the majority of these states lie above the Fermi-level and the emissive copper defects. These conclusions are supported by the large increase in

Please do not adjust margins

QY typically observed in experiment by passivating the surface of CIS with a ZnS shell, which can increase QY by more than 50% after eliminating most electron traps.[9, 15-16] However, the increase in QY does not correspond with a significant change in the Stokes shift or linewidth for CIS QDs indicating that the absorption and emission centers are not simply due to dangling bonds, and are indeed the same or similar to bulk structures. This is consistent with our computational results, which show that Cu defects have a similar affect on the electronic structure of CIS bulk and QD structures. Lastly, the inability to achieve 100% QY from simply shelling CIS with ZnS indicates that surface states are not the *only* source of optical losses in CIS, and other competing bulk-like defects contribute to nonradiative recombination losses. Removal of such defects requires optimizing the stoichiometry and kinetic growth conditions. This, in addition to using a ZnS (or other inorganic) shell to passivate dangling bond surface states can potentially lead to unity quantum yields.

Conclusions

In conclusion, we have identified the stoichiometry- and Fermi-level-dependent formation of defects in CIS QDs, and provided an atomistic rationalization for their unusual optical properties. Anti-site defects are common in (near)-stoichiometric or Cu-rich structures, and lead to intragap excitations that broaden absorption spectra and result in stronger reabsorption losses in LSCs and band-tailing in solid-state solar cells. Copper vacancies are more common in Cu-deficient QDs and are charge-compensated by the oxidation of a second Cu atom. This leads to narrower absorption spectra, DMS characteristics, reduced reabsorption in LSCs, and reduced band-tailing in solar cells. These results help explain several experimental findings.[7, 18, 20, 51] In particular, the "True Stokes shift", which occurs at anti-site defects explains the large Huang-Rhys parameter.[11, 51] However, the occurrence of this shift only at anti-site defects, and the simultaneous presence of delocalized band-edges is still consistent with two-band transient absorption from "Cu^{1+}" defects and narrow single particle emission (~60 meV) broadened by heterogeneity.[7, 18, 20, 56]

Our computational predictions imply that the performance of CIS QDs in energy harvesting applications can be improved by tuning the relative concentration of anti-site defects and copper vacancies through stoichiometry. LSCs and solid-state solar cells utilizing Cu-deficient QDs should have reduced reabsorption and nonradiative recombination losses, and improved scaling of device performance. However, if QDs become *too* Cu-deficient, eventually there will be a reduction in QY due to competition from the $2V_{Cu}'$ + $In_{Cu}^{\bullet\bullet}$ defect phase and/or increased density of electron trapping $In_{Cu}^{\bullet\bullet}$ defects. For near-stoichiometric or Cu-rich CIS, anti-site defect emission can be deactivated by indium or copper vacancies, which leads to lower QY for LSCs and increased nonradiative recombination losses in solid-state solar cells. This, in addition to stronger reabsorption, makes them less ideal for LSCs and solid-state solar cells, but is not as major of a concern for sensitized solar cells where the open-circuit voltage is pinned by the energy difference between the excited-state anti-site defect hole state and the CB electron. Hence, for sensitized solar cells Cu-rich structures may be ideal due to the enhanced sample absorbance from intragap states leading to higher open circuit current density and power conversion efficiency.

Conflicts of interest

There are no conflicts to declare.

Acknowledgements

A.S.F. was supported by the LANL African American Partnership Program. A.N.A. acknowledges the support of the NSF CAREER Award CHE-1351968. All authors thank Victor I. Klimov for thoughtful discussion ~~and for providing the experimental results in ref. 20 prior to publication~~.

Notes and references

1. Brunisholz, M. J. *IEA-PVPS Annual Report* **2016**; Imprimerie St Paul: Fribourg, Switzerland, 2017; ISBN 978-3-906042-63-3.
2. Hallegatte, S. *et al.* Mapping the Climate Change Challenge. *Nat. Climate Change* **2016**, *6*, 663-668.
3. Du, J.; Du, Z.; Hu, J.-S.; Pan, Z.; Shen, Q.; Sun, J.; Long, D.; Dong, H.; Sun, L.; Zhong, X.; Wan, L.-J., Zn–Cu–In–Se Quantum Dot Solar Cells with a Certified Power Conversion Efficiency of 11.6%. *J. Am. Chem. Soc.* **2018,** *138*, 4201-4209.
4. Wang, W.; Zhao, L.; Wang, Y.; Xue, W.; He, F.; Xie, Y.; Li, Y., Facile Secondary Deposition for Improving Quantum Dot Loading in Fabricating Quantum Dot Solar Cells. *J. Am. Chem. Soc.* **2019**, *141*, 4300-4307.
5. Meinardi, F.; McDaniel, H.; Carulli, F.; Colombo, A.; Velizhanin, K. A.; Makarov, N. S.; Simonutti, R.; Klimov, V. I.; Brovelli, S., Highly Efficient Large-Area Colourless Luminescent Solar Concentrators using Heavy-Metal-Free Colloidal Quantum Dots. *Nat. Nanotechnol.* **2015,** *10*, 878-885.
6. Bergren, M. R.; Makarov, N. S.; Ramasamy, K.; Jackson, A.; Guglielmetti, R.; McDaniel, H., High-Performance $CuInS_2$ Quantum Dot Laminated Glass Luminescent Solar Concentrators for Windows. *ACS Energy Lett.* **2018,** *3*, 520-525.
7. Jara, D. H.; Stamplecoskie, K. G.; Kamat, P. V., Two Distinct Transitions in Cu_xInS_2 Quantum Dots. Bandgap versus Sub-Bandgap Excitations in Copper-Deficient Structures. *J. Phys. Chem. Lett.* **2016,** *7*, 1452-1459.
8. Aldakov, D.; Lefrançois, A.; Reiss, P., Ternary and Quaternary Metal Chalcogenide Nanocrystals: Synthesis, Properties and Applications. *J. Mater. Chem. C.* **2013,** *1*, 3756-3776.
9. Berends, A. C.; Rabouw, F. T.; Spoor, F. C. M.; Bladt, E.; Grozema, F. C.; Houtepen, A. J.; Siebbeles, L. D. A.; de Mello Donega, C., Radiative and Nonradiative Recombination in $CuInS_2$ Nanocrystals and $CuInS_2$-Based Core/Shell Nanocrystals. *J. Phys. Chem. Lett.* **2016,** *7*, 3503-3509.
10. van der Stam, W.; de Graaf, M.; Gudjonsdottir, S.; Geuchies, J. J.; Dijkema, J. J.; Kirkwood, N.; Evers, W. H.; Longo, A.; Houtepen, A. J., Tuning and Probing the Distribution of Cu^+ and Cu^{2+} Trap States Responsible for Broad-Band Photoluminescence in $CuInS_2$ Nanocrystals. *ACS Nano* **2018,** *12*, 11244-11253.
11. Knowles, K. E.; Nelson, H. D.; Kilburn, T. B.; Gamelin, D. R., Singlet–Triplet Splittings in the Luminescent Excited States of Colloidal Cu^+:CdSe, Cu^+:InP, and $CuInS_2$ Nanocrystals: Charge-Transfer Configurations and Self-Trapped Excitons. *J. Am. Chem. Soc.* **2015,** *137*, 13138-13147.
12. Hughes, K. E.; Ostheller, S. R.; Nelson, H. D.; Gamelin, D. R., Copper's Role in the Photoluminescence of $Ag_{1-x}Cu_xInS_2$ Nanocrystals, from Copper-Doped $AgInS_2$ ($x \sim 0$) to $CuInS_2$ ($x = 1$). *J. Am. Chem. Soc.* **2019,** *19*, 1318-1325.
13. Nagamine, G.; Nunciaroni, H. B.; McDaniel, H.; Efros, A. L.; de Brito Cruz, C. H.; Padilha, L. A., Evidence of Band-Edge Hole Levels Inversion in Spherical $CuInS_2$ Quantum Dots. *Nano Lett.* **2018,** *18*, 6353-6359.

 This journal is © The Royal Society of Chemistry 20xx

Please do not adjust margins

Please do not adjust margins

14. Berends, A. C.; Mangnus, M. J. J.; Xia, C.; Rabouw, F. T.; de Mello Donega, C., Optoelectronic Properties of Ternary I-III-VI_2 Semiconductor Nanocrystals: Bright Prospects with Elusive Origins. *J. Phys. Chem. Lett.* **2019,** *10*, 1600-1616.
15. Fuhr, A.; Yun, H. J.; Makarov, N. S.; Li, H.; McDaniel, H.; Klimov, V. I., Light-Emission Mechanism in $CuInS_2$ Quantum Dots Evaluated by Spectral Electrochemistry. *ACS Photonics* **2017**, *4*, 2425-2435.
16. Li, L.; Pandey, A.; Werder, D. J.; Khanal, B. P.; Pietryga, J. M.; Klimov, V. I., Efficient Synthesis of Highly Luminescent Copper Indium Sulfide-Based Core/Shell Nanocrystals with Surprisingly Long-Lived Emission. *J. Am. Chem. Soc.* **2011,** *133*, 1176-1179.
17. Rice, W. D.; McDaniel, H.; Klimov, V. I.; Crooker, S. A., Magneto-Optical Properties of $CuInS_2$ Nanocrystals. *J. Phys. Chem. Lett.* **2014,** *5*, 4105-4109.
18. Zang, H.; Li, H.; Makarov, N. S.; Velizhanin, K. A.; Wu, K.; Park, Y.-S.; Klimov, V. I., Thick-Shell $CuInS_2$/ZnS Quantum Dots with Suppressed "Blinking" and Narrow Single-Particle Emission Line Widths. *Nano Lett.* **2017**, *17*, 1787-1795.
19. Pinchetti, V.; Lorenzon, M.; McDaniel, H.; Lorenzi, R.; Meinardi, F.; Klimov, V. I.; Brovelli, S., Spectro-electrochemical Probing of Intrinsic and Extrinsic Processes in Exciton Recombination in I−III−VI_2 Nanocrystals. *Nano Lett.* **2017,** *17*, 4508-4517.
20. Fuhr, A. S.; Yun, H-J.; Crooker, S.; Klimov, V. I. Spectroscopic and Magneto-Optical Signatures of Cu^{1+} and Cu^{2+} Defects in Copper Indium Sulfide Quantum Dots. *ACS Nano* **2020,** DOI:10.1021/acsnano.9b09181.
21. Klimov, V. I.; Baker, T. A.; Lim, J.; Velizhanin, K. A.; McDaniel, H. Quality Factor of Luminescent Solar Concentrators and Practical Concentration Limits Attainable with Semiconductor Quantum Dots. *ACS Photonics* **2016,** *3*, 1138-1148.
22. Knowles, K. E.; Kilburn, T. B.; Alzate, D. G.; McDowall, S.; Gamelin, D. R., Bright $CuInS_2$/CdS Nanocrystal Phosphors for High-Gain Full-Spectrum Luminescent Solar Concentrators. *Chem. Commun.* **2015,** *51*, 9129-9132.
23. Sumner, R.; Eiselt, S.; Kilburn, T. B.; Erickson, C.; Carlson, B.; Gamelin, D. R.; McDowall, S.; Patrick, D. L., Analysis of Optical Losses in High-Efficiency $CuInS_2$-Based Nanocrystal Luminescent Solar Concentrators: Balancing Absorption Versus Scattering. *J. Phys. Chem. C* **2017,** *121*, 3252-3260.
24. Li, C.; Chen, W.; Wu, D.; Quan, D.; Zhou, Z.; Hao, J.; Qin, J.; Li, Y.; He, Z.; Wang, K., Large Stokes Shift and High Efficiency Luminescent Solar Concentrator Incorporated with $CuInS_2$/ZnS Quantum Dots. *Sci. Rep.* **2016,** *5*, 17777.
25. Jara, D. H.; Yoon, S. J.; Stamplecoskie, K. G.; Kamat, P. V., Size-Dependent Photovoltaic Performance of $CuInS_2$ Quantum Dot-Sensitized Solar Cells. *Chem. Mater.* **2014,** *26*, 7221-7228.
26. Panthani, M. G.; Akhavan, V.; Goodfellow, B.; Schmidtke, J. P.; Dunn, L.; Dodabalapur, A.; Barbara, P. F.; Korgel, B. A., Synthesis of $CuInS_2$, $CuInSe_2$, and $Cu(In_xGa_{1-x})Se_2$ (CIGS) Nanocrystal "Inks" for Printable Photovoltaics. *J. Am. Chem. Soc.* **2008,** *130*, 16770-16777.
27. McDaniel, H.; Fuke, N.; Makarov, N. S.; Pietryga, J. M.; Klimov, V. I., An Integrated Approach to Realizing High-Performance Liquid-Junction Quantum Dot Sensitized Solar Cells. *Nat Commun.* **2013,** *4*, 1.
28. McDaniel, H.; Fuke, N.; Pietryga, J. M.; Klimov, V. I., Engineered $CuInSe_xS_{2-x}$ Quantum Dots for Sensitized Solar Cells., *J. Phys. Chem. Lett.* **2013,** *4*, 355-361.
29. Kim, J.-Y.; Yang, J.; Yu, J. H.; Baek, W.; Lee, C.-H.; Son, H. J.; Hyeon, T.; Ko, M. J., Highly Efficient Copper–Indium–Selenide Quantum Dot Solar Cells: Suppression of Carrier Recombination by Controlled ZnS Overlayers. *ACS Nano* **2015,** *9*, 11286-11295.
30. Voggu, V. R.; Sham, J.; Pfeffer, S.; Pate, J.; Fillip, L.; Harvey, T. B.; Brown, R. M.; Korgel, B. A., Flexible $CuInSe_2$ Nanocrystal Solar Cells on Paper. *ACS Energy Lett.* **2017,** *2*, 574-581.
31. Panthani, M. G.; Stolle, C. J.; Reid, D. K.; Rhee, D. J.; Harvey, T. B.; Akhavan, V. A.; Yu, Y.; Korgel, B. A., $CuInSe_2$ Quantum Dot Solar Cells with High Open-Circuit Voltage. *J. Phys. Chem. Lett.* **2013,** *4*, 2030-2034.
32. So, D.; Pradhan, S.; Konstantatos, G., Solid-State Colloidal $CuInS_2$ Quantum Dot Solar Cells Enabled by Bulk Heterojunctions. *Nanoscale.* **2016,** 8 16776-16785.
33. Kresse, G.; Furthmüller, J., Efficiency of Ab-Initio Total Energy Calculations for Metals and Semiconductors using a Plane-Wave Basis Set. *Comput. Mater. Sci.* **1996**, *6*, 15-50.27.
34. Kresse, G.; Furthmüller, J., Efficient Iterative Schemes for Ab Initio Total-Energy Calculations using a Plane-Wave Basis Set. *Phys. Rev. B* **1996**, *54*, 11169-11186.
35. Kresse, G.; Hafner, J., Ab Initio Molecular-Dynamics Simulation of the Liquid-Metal-Amorphous-Semiconductor Transition in Germanium. *Phys. Rev. B* **1994**, *49*, 14251-14269.
36. Kresse, G.; Hafner, J., Ab Initio Molecular Dynamics for Liquid Metals. *Phys. Rev. B* **1993**, 47, 558-561.
37. Heyd, J.; Scuseria, G. E.; Ernzerhof, M., Hybrid Functionals Based on a Screened Coulomb Potential. *J. Chem. Phys.* **2003**, *118*, 8207-8215.
38. Perdew, J. P.; Burke, K.; Ernzerhof, M., Generalized Gradient Approximation Made Simple. *Phys.Rev.Lett.* **1996**, 77, 3865-3868.
39. Freysoldt, C.; Grabowski, B.; Hickel, T.; Neugebauer, J.; Kresse, G.; Janotti, A.; Van de Walle, C. G., First-principles calculations for point defects in solids. *Rev. Mod. Phys.* **2014,** 86, 253.
40. Malitckaya, M.; Komsa, H-P.; Havu, V.; Puska, M., First-Principles Modeling of Point Defects and Complexes in Thin-Film Solar-Cell Absorber $CuInSe_2$ *Adv. Electron. Mater.* **2017,** 3, 1600353.
41. Pohl, J.; Albe, K., Thermodynamics and Kinetics of the Copper Vacancy in $CuInSe_2$, $CuGaSe_2$, $CuInS_2$, and $CuGaS_2$ from Screened-Exchange Hybrid Density Functional Theory. *J. Appl. Phys.* **2010**, *108*, 023509.
42. Chen, H.; Wang, C.-Y.; Wang, J.-T.; Hu, X.-P.; Zhou, S.-X., First-Principles Study of Point Defects in Solar Cell Semiconductor $CuInS_2$. *J. Appl. Phys.* **2012**, *112*, 084513.
43. Le Bahers, T.; Rérat, M.; Sautet, P., Semiconductors Used in Photovoltaic and Photocatalytic Devices: Assessing Fundamental Properties from DFT. *J. Phys. Chem. C* **2014**, 118, 5997-6008.
44. Yamamotoa, Y.; Yamaguchi, T.; Tanaka, T.; Tanahashic, N.; Yoshida, A., Characterization of $CuInS_2$ Thin Films Prepared by Sputtering from Binary Compounds. *Solar Energy Mater. And Solar Cells.* **1997**, *49*, 399-405.
45. Chuang, P.-H.; Lin, C. C.; Liu, R.-S., Emission-Tunable $CuInS_2$/ZnS Quantum Dots: Structure, Optical Properties, and Application in White Light-Emitting Diodes with High Color Rendering Index. *ACS Appl. Mater. Interfaces* **2014,** *6*, 15379-15387.
46. Houck, D. W.; Assaf, E. I.; Shin, H.; Greene, R. M.; Pernik, D. R.; Korgel, B. A., Pervasive Cation Vacancies and Antisite Defects in Copper Indium Diselenide ($CuInSe_2$) Nanocrystals. *J. Phys. Chem. C* **2019,** *123*, 9544-9551.
47. Furdyna, J. K. Diluted Magnetic Semiconductors. *J. Appl. Phys.* **1988**, *64*, R29-R64.
48. Pandey, A; Brovelli, S; Viswanatha, R; Li, L; Pietryga, J. M.; Klimov, V. I.; Crooker, S. A., Long-Lived Photoinduced Magnetization in Copper-doped ZnSe-CdSe Core-Shell Nanocrystals. *Nat Nanotechnol.* **2012**, *7*, 792-797.
49. Bussian, D. A.; Crooker, S. A.; Yin, M.; Brynda, M.; Efros, A. L.; Klimov, V. I., Tunable Magnetic Exchange Interactions in Manganese-Doped Inverted Core–Shell ZnSe–CdSe Nanocrystals. *Nat. Mater.* **2008**, *8*, 35.
50. Shabaev, A.; Mehl, M. J.; Efros, A.I. L., Energy Band Structure of $CuInS_2$ and Optical Spectra of $CuInS_2$ Nanocrystals. *Phys. Rev. B* **2015**, *92*, 035431.
51. Nelson, H. D.; Li, X.; Gamelin, D. R. Computational Studies of the Electronic Structures of Copper-Doped CdSe Nanocrystals: Oxidation States, Jahn–Teller Distortions, Vibronic Bandshapes,

Please do not adjust margins

Please do not adjust margins

and Singlet–Triplet Splittings. *J. Phys. Chem. C* **2016**, *120*, 5714-5723.
52. Long, R.; Prezhdo, O. V., Ab Initio Nonadiabatic Molecular Dynamics of the Ultrafast Electron Injection from a PbSe Quantum Dot into the TiO_2 Surface. *J. Am. Chem. Soc.* **2011**, *133*, 19240-19249.
53. Kim, D.; Kim, D.-H.; Lee, J.-H.; Grossman, J. C., Impact of Stoichiometry on the Electronic Structure of PbS Quantum Dots. *Phys. Rev. Lett.* **2013**, *110*, 196802.
54. Neukirch, A. J.; Hyeon-Deuk, K.; Prezhdo, O. V. Time Domain Ab Initio Modeling of Excitation Dynamics in Quantum Dots. *Coord. Chem. Rev.* **2014**, 263, 161-181.
55. Vörös, M.; Galli, G.; Zimanyi, G., Colloidal Nanoparticles for Intermediate Band Solar Cells. *ACS Nano* **2015**, *9*, 6882-6890.
56. Fuhr, A. S.; Sautet, P.; Alexandrova, A. N., Heterogeneity in Local Chemical Bonding Explains Spectral Broadening in Quantum Dots with Cu Impurities. *J. Phys. Chem. C* **2019,** *123*, 5705-5713.

 This journal is © The Royal Society of Chemistry 20xx

Please do not adjust margins